J. Fluid Mech. (1995), *vol.* 287, *pp.* 59–74

Stokes problems for moving half-planes

By Y. ZENG AND S. WEINBAUM

Department of Mechanical Engineering, The City College of the City University of New York, NY 10031, USA

(Received 24 January 1994 and in revised form 9 September 1994)

New exact solutions of the Navier–Stokes equations are obtained for the unbounded and bounded oscillatory and impulsive tangential edgewise motion of touching half-infinite plates in their own plane. In contrast to Stokes classical solutions for the harmonic and impulsive motion of an infinite plane wall, where the solutions are separable or have a simple similarity form, the present solutions have a two-dimensional structure in the near region of the contact between the half-infinite plates. Nevertheless, it is possible to obtain relatively simple closed-form solutions for the flow field in each case by defining new variables which greatly simplify the r- and θ-dependence of the solutions in the vicinity of the contact region. These solutions for flow in a half-infinite space are then extended to bounded flows in a channel using an image superposition technique. The impulsive motion has application to the motion near geophysical faults, whereas the oscillatory motion has arisen in the design of a novel oscillating half-plate flow chamber for examining the effect of fluid shear stress on cultured cell monolayers.

1. Introduction

Every student of fluid mechanics is familiar with Stokes' celebrated paper on pendulums (1851) in which he describes the now classical problems of the oscillatory and impulsive motion of an infinite plate in its own plane, also known as Stokes problems of the first and second kind. The first problem leads to the planar propagation of a vorticity wave with velocity $c = (2\nu\omega)^{1/2}$ and a penetration depth $\delta = (2\nu/\omega)^{1/2}$, whereas the second has a similarity solution in which the shear stress at the plate decays as $1/t^{1/2}$ and $\delta = 2(\nu t)^{1/2}$. An interesting variation of Stokes first problem has arisen in the design of a novel flow apparatus in which cell tissue monolayers could be subject to spatially non-uniform oscillatory shear. The basic flow geometry is depicted in figure 1(*b*) where a confluent cell tissue monolayer is grown on the top boundary, $y = h$, of a flow channel, whereas the lower boundary, $y = 0$, is a split plate whose right-hand half, $x > 0$, undergoes an impulsive motion or a harmonic oscillation in the z-direction, while its left-hand half remains stationary. This confined parallel channel geometry is the bounded extension of the fundamental problem shown in figure 1(*a*), the edgewise tangential motion of two touching half-infinite plates in the z-direction. The latter is a variation of Stokes first and second problems in which only one half of the plane is moving. The sideways impulsive motion of a half plate is a simple model for the tangential flow parallel to a sudden shearing crack in a surface. Such flows have geophysical applications in earthquakes, fracture of ice sheets and related problems. New exact solutions of the Navier–Stokes equation for the flow in a half space or in a channel under the impulsive and oscillatory driving motions sketched in figures 1(*a*) and 1(*b*) are presented in this study.

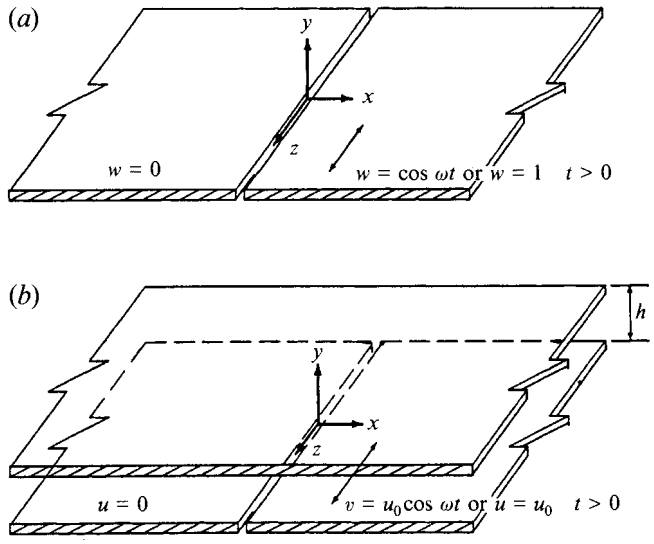

FIGURE 1. The sketches of the flow geometry showing (*a*) flow in a half-plane and (*b*) flow in a channel.

The flow problems in figure 1 are uni-directional flows with a single velocity component in the z-direction that depends on time and the two spatial coordinates in the cross-section of the flow. For these uni-directional flows the nonlinear inertial terms in the Navier–Stokes equations vanish identically and the principal difficulty is the discontinuity in velocity and the singularity in shear stress at $(0, 0)$. We shall show, however, that critical functional simplifications exist in each case and it is possible to obtain closed-form analytic solutions for touching half-infinite plates for both impulsive and harmonic motions. These fundamental solutions are then used to find the solutions for the channel flows in figure 1 (*b*). The latter solutions can be obtained by superposing an infinite series solution derived from a reflection procedure which ensures that the no-slip boundary condition is satisfied on the top wall. Owing to the exponential decay of the fundamental solutions as y increases, the convergence of this superposition is exponentially fast.

The motivation for this study derives from a recent paper by the authors, Weinbaum, Cowin & Zeng (1994), in which a new hypothesis is advanced for the cellular level transduction mechanism by which cells in the mineralized portion of bone, osteocytes, sense mechanical strains due to loading and communicate this loading to the bone forming cells, osteoblasts, at the bone surface. The new hypothesis suggests that the osteocytes, which reside in the fluid filled lacuna–canalicular channels in the bone are biochemically stimulated by mechanically induced fluid shear stresses acting on the membranes of their osteocytic processes. The feasibility of this hypothesis can be tested in cell culture studies in which flow channels are constructed where cultured cell monolayers are subjected to fluid shear stresses in the anticipated physiological range. Extensive studies of this nature have been performed on vascular endothelial monolayers to probe a wide variety of biochemical responses to shear stress since the pioneering study by Dewey *et al.* (1981) first demonstrated the viability of the cells in the shear flow apparatus. In bone, experiments indicate that frequency as well as the magnitude of the mechanical load are important and that the characteristic distance between the surface cells and the most interior osteocytes over which the shear stress varies is typically five cells or approximately 200 μm. The flow apparatus shown

in figure 1(*b*) provides a device wherein the height h can be adjusted to simulate this characteristic distance for cellular shear stress variation and also to reproduce the frequency of physiological loading.

This paper is presented in five sections. Section 2 describes the exact fundamental solutions for the flow in a half-space driven by the tangential edgewise motion of the half-infinite plate shown in figure 1(*a*). The exact solutions for the flow driven by the tangential edgewise motion of the split lower plate in the channel shown in figure 1(*b*) are presented in §3. The results and the discussion of the new solutions are presented in §4 and a brief conclusion is given in §5.

2. Flow driven by an unbounded half-infinite plate

In this section we consider flow in half-infinite space driven impulsively or periodically by the tangential edgewise motion of touching half-infinite plates in the z-direction as sketched in figure 1(*a*). We assume that the only velocity component is parallel to the edge of the plates and thus the x- and y-components of the velocity vanish as in a spatially and temporally varying uni-directional flow in the z-direction. To satisfy continuity velocity component w is independent of z and a function of t, x and y. The governing Navier–Stokes equation for this uni-directional flow is

$$\frac{\partial w}{\partial t} = \nu \nabla^2 w, \tag{1}$$

where ν is the viscosity of the fluid and $\nabla^2 = (\partial^2/\partial x^2) + (\partial^2/\partial y^2)$.

The boundary and initial conditions for the impulsive motion are:

$$w = 0 \quad \text{at } y = 0, \quad x < 0, \quad t > 0 \tag{2a}$$

$$w = 1 \quad \text{at } y = 0, \quad x > 0, \quad t > 0 \tag{2b}$$

$$w = 0 \quad \text{at } t = 0. \tag{2c}$$

The boundary conditions for the oscillatory motion are:

$$w = 0 \qquad \text{at } y = 0, \quad x < 0, \tag{3a}$$

$$w = \cos \omega t \quad \text{at } y = 0, \quad x > 0. \tag{3b}$$

The solutions $w(t, x, y)$ can be decomposed into two parts, w^+ and w^-, one symmetric and the other anti-symmetric in that order about $x = 0$, i.e.

$$w(t, x, y) = \tfrac{1}{2}[w^+(t, y) + w^-(t, x, y)]. \tag{4}$$

The symmetric part w^+ is the classical solution of Stokes for either the impulsive or oscillatory motion of the infinite plate, which are independent of the coordinate x. In the next two subsections we present the fundamental solutions for w^-, for the impulsive and oscillatory driving motions, respectively.

2.1. *Impulsive motion*

In this subsection, we seek a solution for w^- which satisfies equation (1), initial condition (2*c*) and boundary conditions

$$w^- = \pm 1 \quad \text{at } \theta = 0, \pi, \tag{5}$$

where θ is polar angle measured from the x-axis.

The boundary conditions (5) can be made homogeneous by introducing the new variable v'

$$v' = w^- - \left(1 - \frac{2\theta}{\pi}\right), \tag{6}$$

where $1-(2\theta/\pi)$ is the steady state solution for w^- in the upper half-plane which satisfies boundary conditions (5). v' satisfies the initial-value problem:

$$\partial v'/\partial t = \nu \nabla^2 v' \tag{7a}$$

$$v' = 0 \qquad \text{at } \theta = 0, \pi, \quad \text{for } t > 0, \tag{7b}$$

$$v' = -(1-(2\theta/\pi)) \quad \text{at } t = 0. \tag{7c}$$

The solution for v' is not separable because of the θ term in the initial condition (7c). However, one observes that $\partial\theta/\partial x = -(1/r)\sin\theta$, which suggests that although v' is not separable in r and θ, $\partial v'/\partial x$ is. We thus introduce the functional substitution

$$v = \partial v'/\partial x. \tag{8}$$

Taking the x derivative of (7a) and using (8), one obtains

$$\partial v/\partial t = \nu \nabla^2 v, \tag{9a}$$

while (7b) and (7c) become

$$v = 0 \qquad \text{at } \theta = 0, \pi, \quad \text{for } t > 0, \tag{9b}$$

$$v = -\frac{2}{\pi r}\sin\theta \quad \text{at } t = 0. \tag{9c}$$

A separable similarity solution of (9a–c) can now be obtained by seeking a solution of the form $v = -(2/\pi r)\sin\theta f(\eta)$, where η is a similarity variable $\eta = r^2/\nu t$. Substituting this form for v in (9a), one can show that the r- and θ-dependence cancel out of the equation and one is left with the reduced equation,

$$4f''(\eta) + f'(\eta) = 0, \tag{10a}$$

which satisfies the boundary conditions,

$$f(0) = 0, \quad f(\infty) = 1. \tag{10b, c}$$

The solution of (9a–c) is

$$f(\eta) = 1 - \exp(-\tfrac{1}{4}\eta). \tag{11}$$

Thus, the solution of (9a–c) is

$$v = -\frac{2}{\pi r}\sin\theta\left(1 - \exp\left(-\frac{r^2}{4\nu t}\right)\right). \tag{12}$$

Since w^- is antisymmetric about $x = 0$, $w^-(t, 0, y) = 0$. Integrating (8) using solution (12), applying (6) and the foregoing symmetry condition on w^-, one obtains

$$w^- = \frac{2}{\pi}\int_0^x \frac{y}{x'^2 + y^2}\exp\left(-\frac{x'^2 + y^2}{4\nu t}\right)\mathrm{d}x'. \tag{13}$$

Stokes classic solution w^+ for the flow driven by the impulsive motion of an infinite plate is

$$w^+ = 1-\operatorname{erf}\left(\frac{y}{2(\nu t)^{1/2}}\right). \tag{14}$$

Substituting these solutions for w^+ and w^- in (4) one has

$$w = \tfrac{1}{2}-\tfrac{1}{2}\operatorname{erf}\left(\frac{|y|}{2(\nu t)^{1/2}}\right)+\frac{1}{\pi}\int_0^x \frac{|y|}{x'^2+y^2}\exp\left(-\frac{x'^2+y^2}{4\nu t}\right)\mathrm{d}x', \tag{15}$$

where the absolute value | | is used to assure that the solution is valid in the lower half-space where the flow is symmetric about the plane $y = 0$.

If we introduce the dimensionless variables $\xi = x/2(\nu t)^{1/2}$ and $\eta = y/2(\nu t)^{1/2}$, where $\delta = 2(\nu t)^{1/2}$ is the penetration depth, the solution (15) can be written in a dimensionless form

$$w = \tfrac{1}{2}-\tfrac{1}{2}\operatorname{erf}(|\eta|)+\frac{1}{\pi}\int_0^{\xi}\frac{|\eta|}{x'^2+\eta^2}\exp\left(-(x'^2+\eta^2)\right)\mathrm{d}x', \tag{16}$$

which is independent of t. Equation (16) is a similarity solution that depends only on the scaled variables ξ and η since no characteristic length can be defined.

2.2. *Oscillatory motion*

For the oscillatory motion of the right-hand half-plate in figure 1 (*a*) we first introduce the dimensionless variables $\tau = \omega t$, $\xi' = x/(2\nu/\omega)^{1/2}$, $\eta' = y/(2\nu/\omega)^{1/2}$, where $(2\nu/\omega)^{1/2}$ is the penetration depth for Stokes first problem. The dimensionless governing equation and boundary conditions can be written as

$$\frac{\partial w}{\partial t} = 2\nabla^2 w \tag{17a}$$

$$w = 0 \qquad \text{at } \eta' = 0, \quad \xi' < 0, \tag{17b}$$

$$w = \cos\tau \quad \text{at } \eta' = 0, \quad \xi' > 0. \tag{17c}$$

Using the superposition (4), we seek a solution for w^- of the form

$$w^- = \operatorname{Re}\{\exp(\mathrm{i}\tau)v'\}, \tag{18}$$

where v' satisfies

$$\nabla^2 v' = (1+\mathrm{i})^2 v' \tag{19a}$$

$$v' = 1 \qquad \text{at } \eta' = 0, \quad \xi' > 0, \tag{19b}$$

$$v' = -1 \qquad \text{at } \eta' = 0, \quad \xi' < 0, \tag{19c}$$

where $\mathrm{i}^2 = -1$ and $\nabla^2 = (\partial^2/\partial\xi'^2)+(\partial^2/\partial\eta'^2)$.

The solution of (19*a–c*) is non-separable because of inhomogeneity of the boundary conditions. However, the functional substitution $v = \partial v'/\partial\xi'$ significantly simplifies boundary conditions (19*b*, *c*). The resulting governing equation and boundary condition are

$$\nabla^2 v = (1+\mathrm{i})^2 v, \tag{20a}$$

$$v = 2\delta(\xi') \qquad \text{at } \eta' = 0, \tag{20b}$$

where $\delta(\xi')$ is the Dirac delta function. The solution of (20a, b) is

$$v = \frac{2(1+\mathrm{i})}{\pi} K_1((1+\mathrm{i})R)\sin\theta, \tag{21}$$

where K_1 is a modified Bessel function of the second kind, $R = (\xi'^2+\eta'^2)^{1/2}$ and $\tan\theta = \eta'/\xi'$.

Following the same procedure used in deriving (13), one obtains from (6), (8) and (21)

$$w^- = \mathrm{Re}\left[\exp(\mathrm{i}\tau)\frac{2(1+\mathrm{i})}{\pi}\int_0^{\xi'} \frac{\eta'}{(x'^2+\eta'^2)^{1/2}} K_1((1+\mathrm{i})(x'^2+\eta'^2)^{1/2})\,\mathrm{d}x'\right]. \tag{22}$$

The solution (22) describes oscillating half-planes whose motions are 180° out of phase.

Stokes solution w^+ for the infinite oscillating plate is

$$w^+ = \mathrm{Re}[\exp(\mathrm{i}\tau)\exp(-(1+\mathrm{i})|\eta'|)]. \tag{23}$$

Combining (4), (22) and (23) we find

$$w = \mathrm{Re}\left\{\exp(\mathrm{i}\tau)\left[\tfrac{1}{2}\exp(-(1+\mathrm{i})|\eta'|)+\frac{1+\mathrm{i}}{\pi}\int_0^{\xi'} \frac{|\eta'|}{(x'^2+\eta'^2)^{1/2}} K_1((1+\mathrm{i})(x'^2+\eta'^2)^{1/2})\,\mathrm{d}x'\right]\right\}, \tag{24}$$

where $|\,|$ is again used to assure that the solution has the proper symmetry about $y = 0$.

3. Channel flows driven by a moving half-infinite plate

We now consider the channel flows shown in figure 1(b). The governing Navier–Stokes equation is equation (1). The boundary and initial conditions for the impulsive motion are

$$u = 0 \quad \text{at } y = h, \quad |x| < \infty; \quad y = 0, \quad x < 0; \quad t > 0, \tag{25a}$$

$$u = u_0 \quad \text{at } y = 0, \quad x > 0; \quad t > 0, \tag{25b}$$

$$u = 0 \quad \text{at } t = 0, \tag{25c}$$

where h is the height of the channel. The boundary conditions for oscillatory motion are

$$u = 0 \qquad \text{at } y = h, \quad |x| < \infty; \quad y = 0, \quad x < 0, \tag{26a}$$

$$u = u_0\cos\omega t \quad \text{at } y = 0, \quad x > 0. \tag{26b}$$

Note $u(t, x, y)$ is here the velocity component in the z-direction and we have changed notation since the solution for $u(t, x, y)$ will be written in terms of the fundamental solutions $w(t, x, y)$ for a single plane.

In order to satisfy the no-slip boundary conditions on the top wall, $y = h$, we utilize the fundamental solutions derived in the previous section in an infinite series of mirror reflections about the plane $y = h$

$$u(t, x, y) = u_0[w(t, x, y) + \sum_{n=1}^{\infty} w(t, x, y+2nh) - \sum_{n=1}^{\infty} w(t, x, y-2nh)]. \tag{27}$$

Owing to the symmetry of the fundamental solutions (15) and (24) about the plane $y = 0$, $w(t, x, 2nh) = w(t, x, -2nh)$. Thus at $y = 0$

$$u(t, x, 0) = u_0 w(t, x, 0) = \begin{cases} 0 & (x < 0), \\ u_0 & (x > 0), \end{cases} \tag{28}$$

for the impulsive motion and

$$u(t, x, 0) = \begin{cases} 0 & (x < 0), \\ u_0 \cos \omega t & (x > 0), \end{cases} \tag{29}$$

for oscillatory motion. Substituting $n = k-1$ into the first summation in (27), we obtain at $y = h$

$$u(t, x, h) = u_0[w(t, x, h) + \sum_{k=0}^{\infty} w(t, x, (2k-1)h) - \sum_{n=1}^{\infty} w(t, x, -(2n-1)h)] = 0.$$

Therefore, the velocity (27) satisfies the governing equation (1) and boundary conditions on the top and bottom walls for both impulsive and oscillatory flow in the channel.

If we introduce the dimensionless variables $X = x/h$, $Y = y/h$ and substitute (15) in (27), one obtains for the impulsive motion of the lower half-plane

$$\begin{aligned} u(\tau, X, Y)/u_0 = {} & \tfrac{1}{2} + \frac{1}{\pi} \int_0^X \frac{Y}{x'^2 + Y^2} \exp\left(-\frac{x'^2 + Y^2}{4\tau}\right) dx' - \tfrac{1}{2} \operatorname{erf}\left(\frac{Y}{2\tau^{1/2}}\right) \\ & + \sum_{n=1}^{\infty} \left\{ -\frac{1}{2\pi^{1/2}} \left[\operatorname{erf}\left(\frac{y-2n}{2\tau^{1/2}}\right) + \operatorname{erf}\left(\frac{y-2n}{2\tau^{1/2}}\right) \right] \right. \\ & + \frac{1}{\pi} \int_0^x \left[\frac{y+2n}{x'^2 + (y+2n)^2} \exp\left(-\frac{x'^2 + (y+2n)^2}{4\tau}\right) \right. \\ & \left. \left. + \frac{y-2n}{x'^2 + (y-2n)^2} \exp\left(-\frac{x'^2 + (y-2n)^2}{4\tau}\right) \right] dx' \right\}. \end{aligned} \tag{30}$$

As $\tau \to \infty$, the solution (15) for the flow in the unbounded half-space $y > 0$ approaches the steady-state solution

$$w_s^- = 1 - \frac{2\theta}{\pi} = \frac{2}{\pi} \arctan \frac{X}{|Y|}, \tag{31}$$

where the absolute value is again used to assure that the solution is valid in the lower half-space $Y < 0$. Substituting (31) into (27), we obtain

$$u_s^-/u_0 = \frac{2}{\pi} \arctan \frac{X}{Y} + \frac{2}{\pi} \sum_{n=1}^{\infty} \left(\arctan \frac{X}{Y+2n} + \arctan \frac{X}{Y-2n} \right). \tag{32}$$

The solution for steady Couette flow in a channel with $u = u_0$ at $Y = 0$ is

$$u_s^+/u_0 = 1 - Y. \tag{33}$$

Superposing equations (32) and (33), we obtain the asymptotic steady-state solution

$$u_s/u_0 = \tfrac{1}{2}(u_s^+ + u_s^-) = \tfrac{1}{2}(1 - Y) + \frac{1}{2\pi} \arctan \frac{X}{Y} + \frac{1}{\pi} \sum_{n=1}^{\infty} \left(\arctan \frac{X}{Y+2n} + \arctan \frac{X}{Y-2n} \right). \tag{34}$$

For the oscillatory motion of the lower half-plane, one obtains after substituting (24) into (27)

$$u(\tau, X, Y)/u_0 = \mathrm{Re}\Bigg\{\exp(\mathrm{i}\tau)\Bigg[\frac{1}{2}\Bigg(\cosh(1+\mathrm{i})HY - \frac{\cosh(1+1)H}{\sinh(1+\mathrm{i})H}\sinh(1+\mathrm{i})HY\Bigg) + \frac{(1+\mathrm{i})H}{\pi}\int_0^X \frac{Y}{x'^2+Y^2}K_1((1+\mathrm{i})H(x'^2+Y^2)^{1/2})\,\mathrm{d}x' + \frac{(1+\mathrm{i})H}{\pi}\int_0^X \sum_{n=1}^{\infty}\Bigg(\frac{Y+2n}{(x'^2+(Y+2n)^2)^{1/2}}K_1((1+\mathrm{i})H(x'^2+(Y+2n)^2)^{1/2}) + \frac{Y-2n}{(x'^2+(Y-2n)^2)^{1/2}}K_1((1+\mathrm{i})H(x'^2+(Y-2n)^2)^{1/2})\Bigg)\mathrm{d}x'\Bigg]\Bigg\}, \tag{35}$$

where $H = h/(2\nu/\omega)^{1/2}$ is the scaled channel height.

The shear stress acting on the top wall $Y = 1$ is given by

$$s_1 = \mu\frac{\partial u}{\partial y}\Big|_{Y=1} = \frac{\mu u_0}{h}\mathrm{Re}\{\exp(\mathrm{i}\tau)[U+\mathrm{i}V]\} = \frac{\mu u_0}{h}\mathrm{Re}\Bigg\{\exp(\mathrm{i}\tau)\Bigg[-\frac{(1+\mathrm{i})H}{2\sinh(1+\mathrm{i})H} + \frac{2(1+\mathrm{i})H}{\pi}\int_0^X \sum_{n=1}^{\infty}\Bigg(\frac{1}{(x'^2+(2n-1)^2)^{1/2}}K_1((1+\mathrm{i})H(x'^2+(2n-1)^2)^{1/2}) - \frac{(1+i)H(2n-1)^2}{x'^2+(2n+1)^2}K_2((1+\mathrm{i})H(x'^2+(2n-1)^2)^{1/2})\Bigg)\mathrm{d}x'\Bigg]\Bigg\}. \tag{36}$$

The maximum value of the stress during a temporal cycle is reached when $\tau = \tau_{max} = -\tan^{-1}(V/U)$, where U and V are defined in (36). At this value of τ, the maximum dimensionless stress $\bar{s}_{max}$ is given by

$$\bar{s}_{max} = \frac{s_{max}}{\mu u_0/h} = (U^2+V^2)^{1/2}. \tag{37}$$

The dimensionless maximum shear stress acting on the top wall $Y = 1$ is

$$\bar{s}_{max_1} = \Bigg|-\frac{(1+\mathrm{i})H}{2\sinh(1+\mathrm{i})H} + \frac{2(1+\mathrm{i})H}{\pi}\int_0^X \sum_{n=1}^{\infty}\Bigg[\frac{K_1((1+\mathrm{i})H(x'^2+(2n-1)^2)^{1/2})}{(x'^2+(2n-1)^2)^{1/2}} - \frac{(1+\mathrm{i})H(2n-1)^2}{x'^2(2n-1)^2}K_2((1+\mathrm{i})H(x'^2+(2n-1)^2)^{1/2})\,\mathrm{d}x'\Bigg]\Bigg|. \tag{38}$$

The first term in (38) is half the dimensionless maximum shear stress $\bar{s}_{max\,1\infty}$ acting on the top wall $Y = 1$ for an infinite-plane oscillation.

The maximum shear stress acting on the bottom wall $Y = 0$ is evaluated using the same procedure outlined for the derivation of (38),

$$\bar{s}_{max_2} = \Bigg|-\frac{(1+\mathrm{i})H}{2\tanh(1+\mathrm{i})H} + \frac{2(1+\mathrm{i})H}{\pi}\int_0^X \sum_{n=1}^{\infty}\Bigg[\frac{K_1((1+\mathrm{i})H(x'^2+4n^2)^{1/2})}{(x'^2+4n^2)^{1/2}} - \frac{(1+\mathrm{i})H4n^2}{x'^2+4n^2}K_2((1+\mathrm{i})H(x'^2+4n^2)^{1/2})\Bigg]\mathrm{d}x' + s_0\Bigg|, \tag{39}$$

where
$$s_0 = \frac{1}{2}\frac{\partial v'(X, Y)}{\partial Y}\bigg|_{Y=0}. \tag{40}$$

The first term in (40) is half the maximum shear stress acting on the bottom wall for an infinite-plane oscillating at $Y = 0$.

To determine s_0 in (40) we first note that

$$v'(X, Y) = \begin{cases} -\dfrac{2(1+\mathrm{i})H}{\pi}\displaystyle\int_X^{+\infty} \frac{|Y|}{(x'^2+Y^2)^{1/2}} K_1((1+\mathrm{i})H(x'^2+Y^2)^{1/2})\,\mathrm{d}x' + v'(+\infty, Y) \\ \qquad\qquad\qquad\qquad\qquad\qquad\qquad\qquad \text{for } X > 0, \\ \dfrac{2(1+\mathrm{i})H}{\pi}\displaystyle\int_{-\infty}^{X} \frac{|Y|}{(x'^2+Y^2)^{1/2}} K_1((1+\mathrm{i})H(x'^2+Y^2)^{1/2})\,\mathrm{d}x' + v'(-\infty, Y) \\ \qquad\qquad\qquad\qquad\qquad\qquad\qquad\qquad \text{for } X < 0. \end{cases} \tag{41}$$

From (18) and the symmetry and asymptotic properties of w^-, one can see

$$v'(+\infty, Y) = -v'(-\infty, Y) = \exp(-(1+\mathrm{i})H|Y|).$$

Thus, (41) becomes

$$v'(X, Y) = \frac{|X|}{X}\left[\exp(-(1+\mathrm{i})H|Y|) - \frac{2(1+\mathrm{i})H}{\pi}\int_{|X|}^{\infty} \frac{|X|}{(x'^2+Y^2)^{1/2}} K_1((1+\mathrm{i})H(x'^2+Y^2)^{1/2})\,\mathrm{d}x'\right],$$

and s_0 from (40) is given by

$$s_0 = -(1+\mathrm{i})H\frac{|X|}{X}\left[\frac{1}{2} + \frac{1}{\pi}\int_{|X|}^{\infty} \frac{K_1((1+\mathrm{i})Hx')}{x'}\,\mathrm{d}x'\right]. \tag{42}$$

4. Results and discussion

The single integrals in the solutions for the velocity field for the single plane motions, equations (15) and (24), have been evaluated numerically. For the channel-flow problems, we require that the error in the truncated infinite series in (30), (34) and (35) be less than 10^{-4}.

The velocity profiles at ξ or $\xi' = -1, -0.1, -0.01, 0, 0.01, 0.1, 1$ and ∞, for the flow in the upper half-space for the impulsive and oscillatory motion of a single split plate are plotted in figures 2(*a*) and 2(*b*), respectively. The profiles for the oscillatory motion are shown at $\omega t = 0$. The figures show that the point $(0, 0)$ is a singular point and the profiles at $\xi = 0$ are a dividing line above which the profiles ($\xi > 0$) asymptotically approach Stokes classical solutions for the infinite-plane motions and below which the profiles ($\xi < 0$) decay with distance from $\xi = 0$. The oscillatory profiles show the propagation of a vorticity wave which is nearly completely damped out for $\xi < -1$. The decay in the amplitude of the boundary motion is thus much more rapid in the x-direction than in the y-direction where there is a significant disturbance at $\eta = 1$. This asymmetry illustrates the importance of two-dimensional effects in the region $R < 1$.

Figures 3(*a*) and 3(*b*) show the velocity profiles at different cross-sections, $X = -1$,

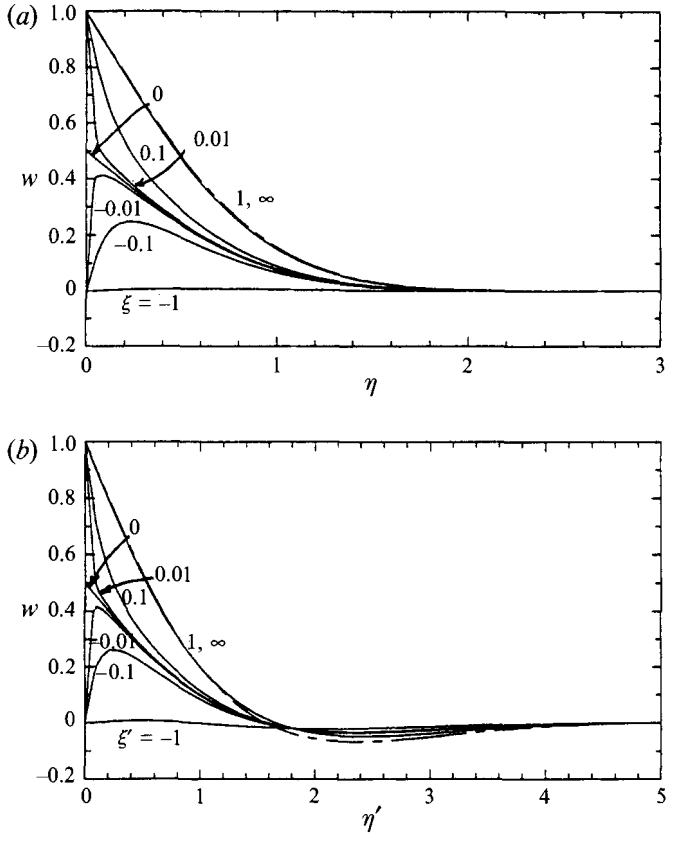

FIGURE 2. Velocity profiles, equations (16) and (24), at different sections, $\xi = -1$, -0.1, -0.01, 0, 0.01, 0.1, 1 and ∞, for flow in upper half space driven by the impulsive and oscillatory motion of a right half-plane when the left half-plane is stationary. The phase for the oscillatory motion is $\omega t = 0$.

-0.1, -0.01, 0, 0.01, 0.1, 1 and ∞, for flow in a channel driven by a half-infinite impulsive moving plate at $\nu t/h^2 = 0.01$ and 0.1, respectively. Figure 3(*c*) shows the asymptotic steady-state velocity profiles at the same cross-sections for steady flow in a channel whose lower right-hand half boundary is moving at constant velocity u_0, whereas figures 4(*a*)–4(*c*) show the corresponding velocity profiles at the same cross-sections at $\omega t = 0$ for the flow in a channel driven by a half-infinite oscillating plate as the scaled channel height $H = h/(2\nu/\omega)^{1/2} = h/\delta$ is increased from 1 to 3 to 10, in that order. These profiles show the important difference in the influence of the upper boundary in the two problems. Both solutions asymptotically tend to the classic bounded whole-plane driven solutions as $x \to \infty$. (0, 0) is a singular point where the velocity is discontinuous. For the case of impulsive motion when $\tau = \nu t/h^2 = 0.01$ (figure 3*a*) the influence of the singular point is confined to a local region that is a small fraction of the channel height and the solution exhibits a behaviour that is very similar to the unbounded solution in figure 2(*a*). As the vorticity fills the channel an asymptotic steady state is achieved. The profiles for $\tau > 0.3$ (not shown) are nearly the same as those shown in figure 3(*c*) for $\tau = \infty$, indicating that steady state is achieved for practical purposes in a time $t = 0.3h^2/\nu$. The effect of the singular point is confined to the region $|X| < 1$ for all t.

The behaviour for the oscillatory flow in figure 4 is somewhat more complicated since a second characteristic length $\delta = (2\nu/\omega)^{1/2}$, the penetration depth, appears. The

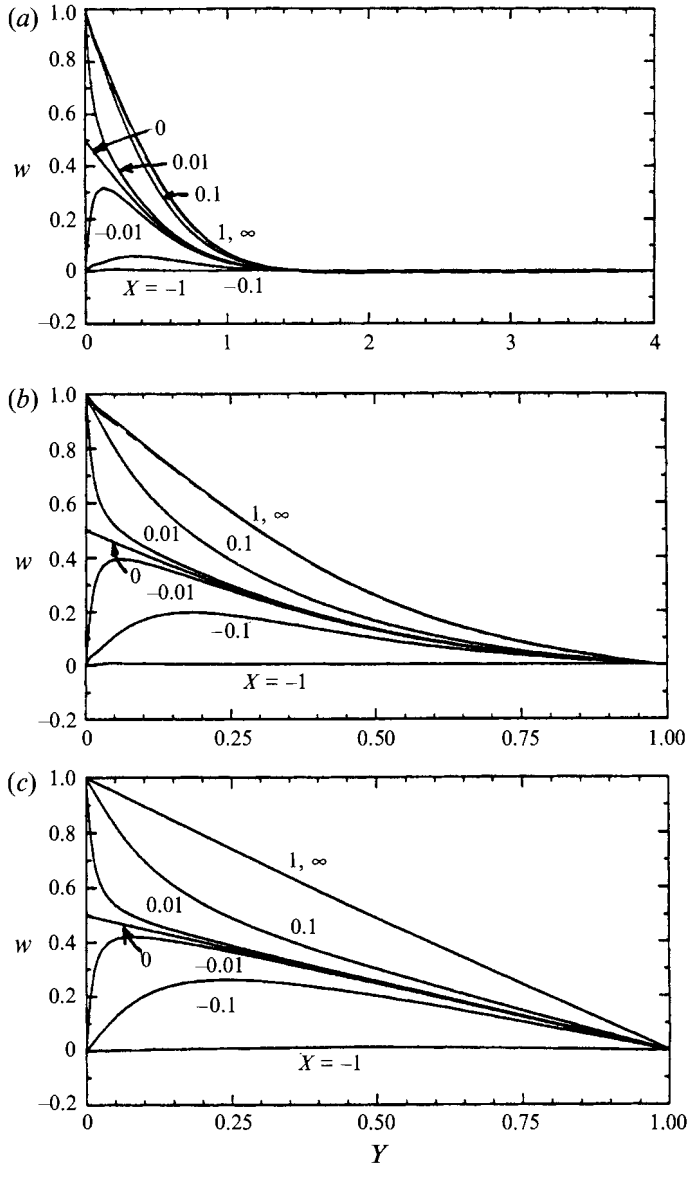

FIGURE 3. (*a*, *b*) Velocity profiles, equation (30), for flow in a channel driven by a half-infinite impulsive moving plate at cross-sections, $X = -1, -0.1, -0.01, 0, 0.01, 0.1, 1$ and ∞, for impulsive motion at $\nu t/h^2 = 0.01$, and 0.1 respectively. (*c*) Asymptotic steady state velocity profiles, equation (34), at the same cross-sections for steady flow in a channel whose lower right-half boundary is moving at constant velocity u_0.

solutions exhibit different behaviour depending on the dimensionless height parameter $H = h/\delta$. For $H = 1$ (figure 4*a*) one observes quasi-steady oscillations that are nearly damped out for $X = x/h < -1.0$. The profiles for $H < 1$ are nearly indistinguishable from those in figure 4(*a*). For $H = 3$, a propagating vorticity wave appears (figure 4*b*). For $H = 10$ (figure 4*c*) the flow has a boundary-layer like structure near the oscillating lower half-plate. The lateral influence of the singularity is confined to the region $|X| < 0.1$ when $H = 10$.

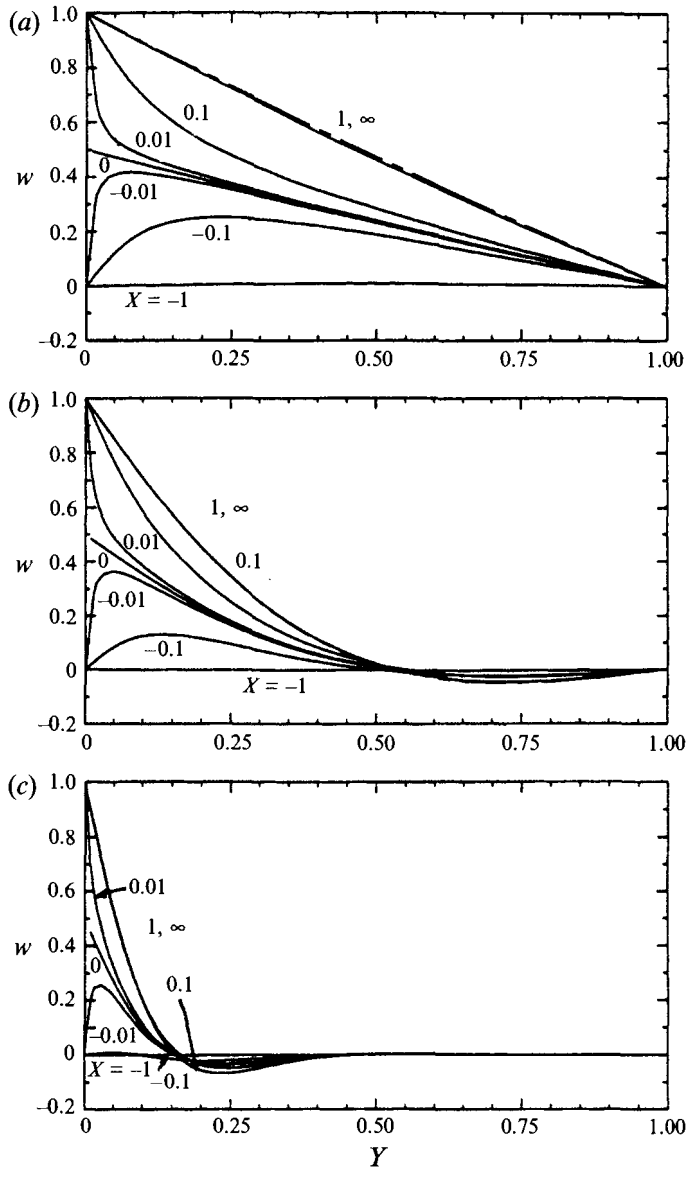

FIGURE 4. Velocity profiles for the oscillating flow in a channel, equation (35), at cross-sections, $X = -1$, -0.1, -0.01, 0, 0.01, 0.1, 1 and ∞, corresponding to phase $\omega t = 0$ at (*a*) $H = 1$, (*b*) $H = 3$ and (*c*) $H = 10$.

Figures 5(*a*) and 5(*b*) show the equi-velocity contours for the flow in a channel driven by a half-impulsive moving plate at $\nu t/h^2 = 0.01$ and 0.1, corresponding to the velocity profiles in figures 3(*a*) and 3(*b*), respectively. The equi-velocity contours for the oscillatory half-plane flow in a channel are omitted to save space but are similar to figures 5(*a*) and 5(*b*) if $(\nu t)^{1/2}/h$ is replaced by the parameter $\delta/h = (2\nu/\omega)^{1/2}/h = H^{-1}$.

Figures 6(*a*) and 6(*b*) are plots of the maximum dimensionless shear stress distribution along the top and bottom walls during a temporal cycle for the half-plane oscillatory channel flow, equations (38) and (39). The figures reveal that there is little change in the maximum shear stress distribution at the upper and lower boundaries for

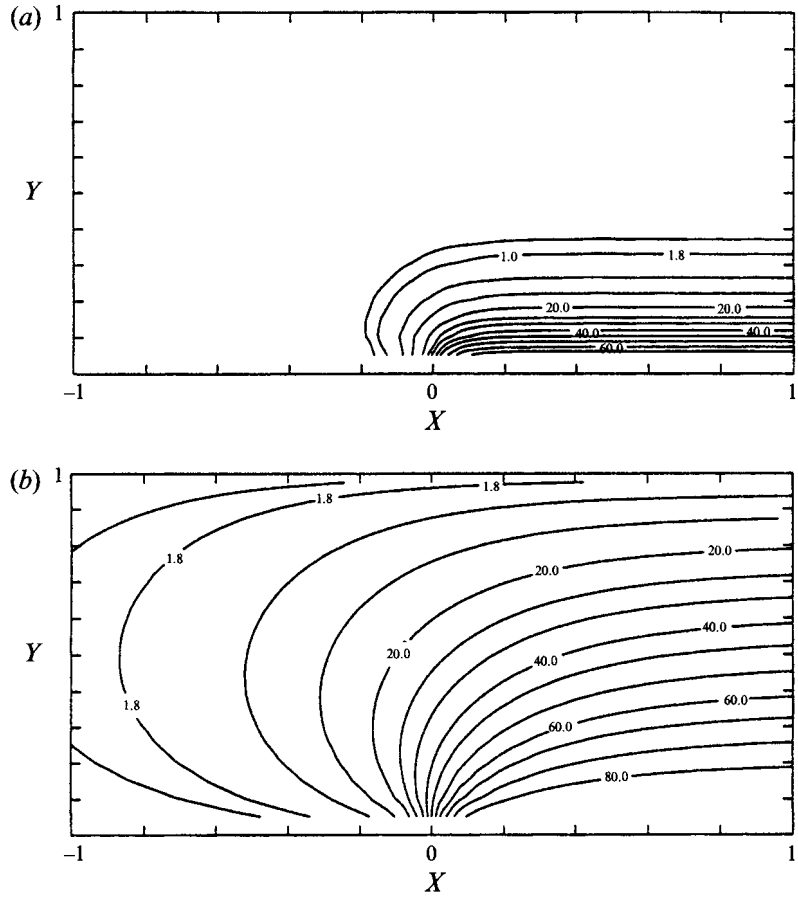

FIGURE 5. Equi-velocity contours for flow in a channel driven by a half-infinite impulsive moving plate, equation (30), at $\nu t/h^2 = 0.01$ and 1, respectively, with the real values 10^{-2} times the labelled ones.

$H \leqslant 0.5$. For these values of H the velocity profiles change in a quasi-steady manner (see figure 4*a*) since the frequency is low enough for the vorticity to diffuse to both boundaries. For $H > 5$, the propagating vorticity wave has been nearly damped out at the upper boundary and $\bar{s}_{max_1} < 0.1$. For $X \gg 1$, $\bar{s}_{max_1}$ approaches the asymptotic limiting value $\sqrt{2}\, H/|\sinh(1+\mathrm{i})\, H|$ given by twice the first term in (38). In contrast to these results at the upper wall, the maximum shear stress distribution at the lower boundary decreases monotonically for $X < 0$ as H increases, whereas it increases for $X > 0$ as H increases. One notes that for $H \geqslant 3$ there is a minimum which is slightly less than the asymptotical value $\sqrt{2}\, H/|\tanh(1+\mathrm{i})\, H|$ for $X \gg 1$. The shear stress is singular at $X = 0$ and the region of influence of the singularity is confined to a distance of order $|X| = H^{-1}$.

The infinite shear stress at the origin leads to an infinite force on the oscillating plates. This is a physically unrealizable behaviour since there must always be some small, but finite, gap of half-width Δ between the plates. We have examined this limiting behaviour by looking at two zero thickness half-plates in which the fluid above and below the half plates is connected by a narrow infinite slit of width 2Δ. The flow is then divided into two regions, an outer region which is described by the asymptotic solution in this paper and an inner region which is defined by the dimensionless length

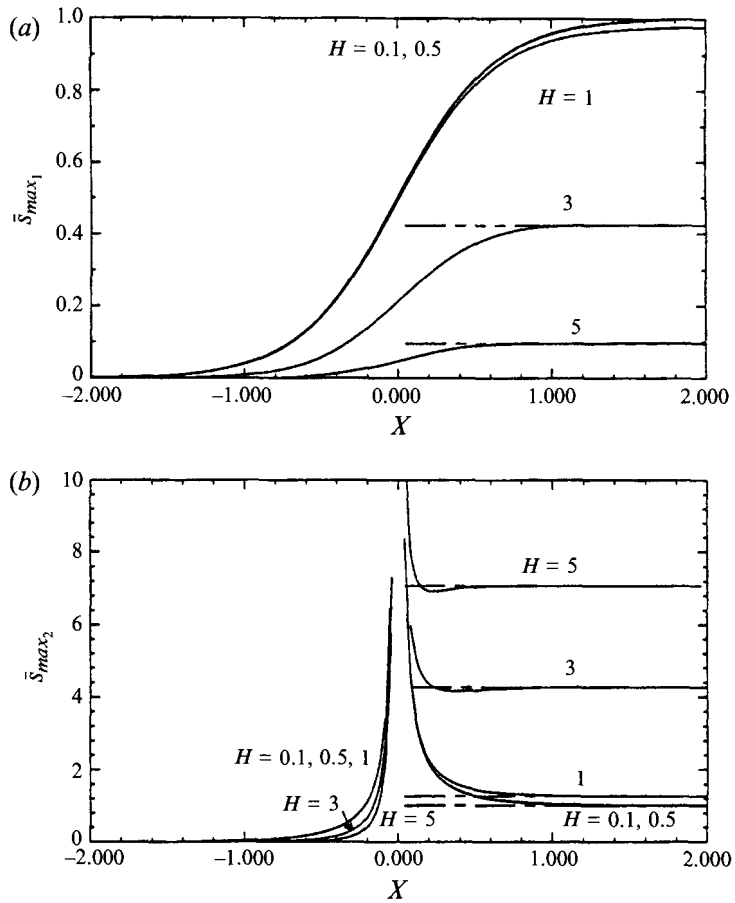

FIGURE 6. The dimensionless maximum shear stresses $\bar{s}_{max_1}$ and $\bar{s}_{max_2}$, equations (38) and (39), acting on the top and bottom walls for oscillating flow in a channel for representative dimensionless heights $H = 0.1$, 0.5, 1, 3 and 5. Dashed lines asymptotic limiting maximum shear stress for infinite lower plate oscillation.

parameter $\Delta^2/(2\nu/\omega) \ll 1$. In this inner region one can show from asymptotic analysis that the governing equation (19*a*) reduces to Laplace's equation, the flow to leading order is quasi-steady and the boundary conditions are given by (19*b*) and (19*c*) for $x' = x/\Delta > 1$ or < -1 in that order. The solution to this inner boundary-value problem can be obtained by conformal mapping (Joukowski transformation). The velocity and shear stress for this solution are bounded in the inner region. We give only the final result for the shear stress at the top or bottom of the half-plates (the details of this solution can be obtained by writing to the authors)

$$s = \frac{2\mu}{\pi\Delta}\left[\frac{1+x'(x'^2-1)}{|x'+(x'^2-1)^{1/2}|}\right] \quad (x' > 1, x' < -1). \tag{43}$$

In the limit $x' \to \pm 1$, (43) reduces to $s = \pm 2\mu/(\pi\Delta)$. If one now examines the behaviour of the outer solution for the shear stress derived from (35) in the limit as $x \to 0$, one finds that s is now given by this same limiting form for (43) as $x' \to \pm 1$, but with Δ replaced by x and the signs reversed. Thus, in the limit $\Delta \to 0$ the singularity can be removed by adding the inner and outer solutions and a finite integral obtained for the force on the walls.

The stability of time periodic Stokes layers is reviewed in Davis (1976). The criteria for the stability of these layers depend on two parameters, the quantity H describing the ratio of the channel height h to the viscous penetration depth δ and the Reynolds number $R^{\omega} = U\delta/\nu$ defined by the amplitude of the plate velocity and the penetration depth. One might anticipate that Stokes layers might be unstable because the velocity profile is highly inflexional. Both energy analysis using Floquet theory for finite-amplitude disturbances and linear stability theory for infinitesimal disturbances have shown that Stokes layers are surprisingly stable except for the case where the wall streamlines are curved and periodic axial vortices of the Taylor–Görtler type are possible, Hall (1984). Although the w velocity component is two-dimensional in the present solution, the streamlines are straight and thus one would intuitively expect the stability to be determined by similar criteria to those studied for traditional Stokes layers with straight streamlines.

In the traditional analysis of Stokes layers with straight streamlines, one finds from linear analysis (evolution of disturbances over a cycle) that the basic flow is stable for $R^{\omega} < 800$ for $H = 8$ and this critical Reynolds number increases as H increases (von Kerczek & Davis 1974). The more unstable part of the flow is associated with the inflexional points in the nearly motionless fluid outside of the Stokes layer where the effects of the boundaries do not damp the infinitesimal disturbances. By this same reasoning, the boundary dominated quasi-steady inner region should be stable and the more 'dangerous' part of the flow should be the inviscid instability associated with the inflexion points in the velocity profiles in the outer region. The unusual stability of these instantaneous inflexion points can be explained by the fact that they propagate away from the boundary too quickly to allow the growth of local instabilities.

In our final remarks we return to the design of the novel flow chamber that motivated this study. Bone cells are typically subject to mechanically induced shear flows at either 1 Hz due to locomotion or 15–25 Hz due to muscular contractions required to maintain posture. In our flow chamber a cell culture monolayer is grown to confluence on the upper boundary of the channel and the channel height h and characteristic velocity u_0 are chosen to simulate a physiological shear stress which is of the order of 10 dynes cm^{-2}. For water ($\mu = 10^{-2}$ dynes cm^{-2} s^{-1}) and a typical channel height of 200 μm this is achieved for $u_0 = 20$ cm s^{-1}. For these values one finds that $H = 0.7$ for $\omega = 20$ Hz and $H = 0.15$ for $\omega = 1$ Hz. The maximum shear stress distribution on the upper boundary is therefore given by the curves for $H < 1$ in figure 6(*a*). As already discussed for these profiles the shear rises from zero to a maximum, $\bar{s}_{max_1} \approx 1.0$, over a region, $|X| < 1$. For these values of H, inertia effects are very small even at $\omega = 20$ Hz. This shear stress distribution closely mimics the physiologically predicted loading of osteons and trabecular elements in the recently developed poroelastic lacunar–canalicular model of Weinbaum *et al.* (1994). The proposed flow chamber is thus able to replicate both the characteristic lengthscale and the frequency variation of the fluid shear stress distribution on the membranes of the osteocytic processes in the canaliculi.

5. Conclusion

In summary we have obtained new exact solutions of the Navier–Stokes equation for flows driven by the impulsive and oscillatory motion of bounded or unbounded touching half-planes. The solutions for a single split-plane motion in a half-space show the transition to the classical infinite-plane solutions of Stokes as X increases. The flow driven by the impulsive motion of a bounded half-plane reaches its steady state in a

time of order $\nu t/h^2 \sim 0.3$. The two-dimensionality of the oscillatory solution is confined to a region of order $\delta = (2\nu/\omega)^{1/2}$ about the point of contact between the moving and stationary half-planes. The maximum shear stress acting on the bottom wall during a cycle is singular as one approaches the contact point while that on the top wall decreases exponentially as $H = h/\delta$ increases.

The authors would like to thank Professor S. C. Cowin for his helpful comments. This research is supported by NASA grant NAGW 2860.

REFERENCES

DAVIS, S. H. 1976 The stability of time-periodic flows. *Ann. Rev. Fluid Mech.* **8**, 57–74.

DEWEY, C. F., BUSSOLARI, S. R., GIMBRONE, M. A. & DAVIES, P. F. 1981 The dynamic response of vascular endothelial cells to fluid shear stress. *Trans. ASME* K: *J. Biomech. Engng* **103**, 177–181.

HALL, P. 1984 On the stability of the unsteady boundary layer on a cylinder oscillating transversely in a viscous fluid. *J. Fluid Mech.* **146**, 347–367.

KERCZEK, C. VON & DAVIS, S. H. 1974 Linear stability theory of oscillating Stokes layers. *J. Fluid Mech.* **62**, 753–773.

STOKES, G. G. 1851 On the effect of internal friction of fluids on the motion of pendulums. *Trans. Camb. Phil. Soc.* **9**, 8–106.

WEINBAUM, S., COWIN, S. C. & ZENG, Y. 1994 A model for the excitation of osteocytes by mechanical loading induced bone fluid shear stress. *J. Biomech.* **27**, pp. 339–360.